Coherent imaging of periodic thick fine isolated structures

J. T. Sheridan and C. J. R. Sheppard*

Angewandte Optik, Physikalisches Institut, University of Erlangen-Nuremberg, Staudtstrasse 7/B2, D-8520 Erlangen, Germany

Received March 18, 1992; revised manuscript received September 14, 1992; accepted September 30, 1992

The diffraction orders and coherent bright and dark field images produced by isolated steps and grooves (notches and trenches) are examined. The isolated structures are approximated by means of a grating with a large period that contains small, widely separated, lamellar structures. The rigorous modal method for TE polarized incident light is used for the numerical calculations. Structures in two types of dielectric material, refractive index $n = 1.5$ and $n = 4.0$, are discussed. The images are examined for variations with several parameters, including width and thickness of the structure and focus position. Several approximate methods for calculating these images, based on first-order approximations, are suggested.

1. INTRODUCTION

The manufacture and use of optically thick, fine structures, both as diffraction gratings and in the semiconductor industry, are of ever-increasing importance. Optical metrology offers significant advantages to those interested in both the design and quality control of such structures. Despite a limited resolution, the technique is popular because it is a familiar, inexpensive, nondestructive, and fast means of acquiring structural information in the form of images. Although images of semitransparent objects have received much attention,[1] thick objects, in which multiple scattering occurs, have received less because of their inherent complexity.

Many exotic modes and geometries of optical microscopy, including scanning confocal[2,3] and coherence probe[4] approaches may be employed to image trenches and steps; however, simple coherent illumination is commonly used in optical metrology of fine line structures. It is often important with structures resulting from semiconductor microlithography, for example, to extract accurate information about the structure's dimensions. The task is difficult when the structures are fine compared with the wavelength of the incident light. Any study of line structures that sheds light on the variation of the diffracted orders above the structure with various parameters, e.g., thickness, width, and material, would be of great practical use.

Line structures are rarely periodic and in many cases are less than 1 μm wide or of the order of one wavelength of the incident radiation. In many cases the feature to be examined is an isolated dielectric step or groove upon a dielectric substrate. To increase the information available from the images of thick structures, a precise model must be available to aid in the interpretation of the result. In this paper we closely examine the variation of the images of two common forms of isolated dielectric structure for changes of period, thickness, and focus position; we use the results from the rigorous modal method.

Many different rigorous methods have been used to calculate the diffraction orders resulting from dielectric and metallic surface-relief gratings.[5-9] Two of these methods, the modal method[10] and the coupled-wave method,[11] were examined previously.[12] Both methods encounter numerical difficulties in convergence and accuracy, especially for gratings of large period or made of lossy material. Difficulties are also encountered for illumination at large angles of incidence. It was concluded, however, that the modal method is the superior of the two numerically for surface-relief gratings.[12]

Calculations of the coherent images of phase and lossy microstructures were carried out previously by Nyyssonen.[13] The one-dimensional waveguide modal method of Burckhardt[10] and Kaspar[14] was employed and extended to the imaging of nonuniform periodic gratings.[15,16] For the numerical reasons mentioned above the technique has not been applied for large cones of incidence, and neither polarization effects nor nonperiodic gratings have been considered in detail. Effects from a large numerical aperture require treatment similar to that of Richards and Wolf.[17] Yuan *et al.*[18] used a modified form of the modal method successfully to extend the method to predict differential Normarski images that account for polarization effects and higher numerical apertures.

Previously[12,19,20] the diffraction orders from two forms of dielectric square-wave surface-relief gratings were examined, and a discussion of the coherent images of these structures was undertaken.[21] However, in all cases the periods examined were greater than 10λ, and so the structure was large; the aim in these cases was to examine the effects of isolated edges. The imaging of isolated grooves or steps that are fine compared with the incident light should reveal new information about the imaging of fine structures. Both isolated grooves and steps will be examined. In both cases the width of the step or groove will be assumed to be in the range between 0.5λ and 4.0λ. Two common physical geometries of gratings, denoted G1 and G2, will be examined as shown in Fig. 1.

Generation of the theoretical images requires three steps. First, a period must be found to ensure that the effects of adjoining steps or grooves are minimized. Second, the number of terms included in the permittivity expansion, and so in the modal expansion of the E field in the grating, must be chosen so that optimum convergence

0740-3232/93/040614-19$05.00

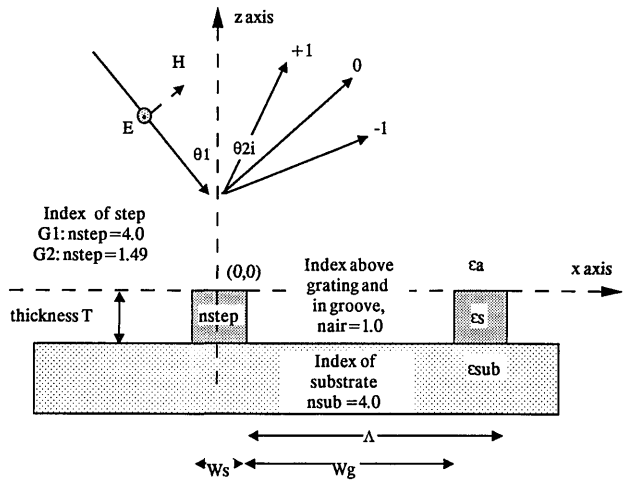

Fig. 1. Two dielectric structures examined, G1 and G2, with TE polarized incident light. In all the cases examined, $\theta_1 = 0$, and the orders will be arranged symmetrically above the structure with the zero order traveling back up the input beam. For isolated steps $W_g \gg W_s$ and for isolated grooves $W_s \gg W_g$.

can be achieved. Finally, comparisons of the effects of a set of parameters including the numerical aperture (NA), the defocus position, and the use of bright field (BF) or dark field (DF) imaging will be examined. Since the zeroth order in most cases dominates the results, calculations of the DF images seems appropriate. It is in fact hoped that examination and comparison of both coherent DF and BF images will provide all the metrological information necessary about small surface-relief structures.

2. APPLICATION OF THE RIGOROUS MODAL METHOD

Diffraction by the structure is calculated from the rigorous modal method. Starting with the Helmholtz, or scalar wave, equation for the TE polarized E field inside the grating,

$$\nabla^2\mathbf{E}(x,z) + k^2\epsilon(x)\mathbf{E}(x,z) = 0, \tag{1}$$

where $k = 2\pi/\lambda$. We use the Fourier series to expand the permittivity of the grating:

$$\epsilon(x) = \epsilon_0 + \sum_{n=1}^{\infty} \hat{\epsilon}_n \cos(nKx), \tag{2}$$

where $K = 2\pi/\Lambda$ and the coefficients for the structures shown in Fig. 1 are given by

$$\epsilon_0 = \frac{1}{\Lambda}(\epsilon_a W_g + \epsilon_s W_s), \tag{3}$$

$$\hat{\epsilon}_n = \frac{2}{n\pi}(\epsilon_a - \epsilon_s)\sin(n\pi W_g/\Lambda), \tag{4}$$

with ϵ_a the permittivity of air, ϵ_s the permittivity of the dielectric in the step, W_g the width of the gap, W_s that of the step, and all the other variables as shown in Fig. 1. We then use the principle of the separation of variables to split the E field within the grating into two orthogonal sets of modes:

$$E_g(x,z) = X(x)Z(z). \tag{5}$$

Application of the boundary conditions permits the removal of all unknowns[12] and permits the calculation of all the wave amplitudes traveling externally to the grating.

There are many difficulties in the numerical implementation of the modal method. Computer time and memory space are two obvious problems, as are testing for and achieving convergence. The difficulties are compounded by such theoretical difficulties as the Gibbs phenomenon[21-25] and the existence of Woods anomalies.[26] All these inherent problems encourage the use of simpler approximate models wherever possible. Because the structures that are of importance to our examination are so small, models based on the Fresnel coefficients are not really acceptable. However, at this stage only some simple first-order approximate models will be suggested.

3. COHERENT IMAGING INTEGRAL

The diffraction orders, once calculated, can then be combined to produce various forms of images of the structure under examination. This paper deals with the simplest theoretical type of illumination and collection. The structures are illuminated normally with coherent light, and the beams traveling in the reflected direction, within the aperture of a cylindrical lens, are collected. Thus no skew waves are included in the calculation, and essentially a line object is imaged.

The image amplitude in such a conventional coherent reflection geometry system with TE polarized light incident at an angle θ_1 is given by

$$U(x,z) = \int_{-\alpha}^{+\alpha} s(\theta_1,\theta_2)P_2(\theta_2)\exp\{+jk[\sin(\theta_1) + \sin(\theta_2)]x\} \times \exp\{+jk[\cos(\theta_1) + \cos(\theta_2)]z\}d\theta_2, \tag{6}$$

where the pupil function $P_2(\theta_2)$ of the objective includes the aplanatic factor[17] $\cos^{1/2}(\theta_2)$. In Eq. (6) θ_2 is the angle of the output beam and α is the aperture of the imaging system. We use the modal method to calculate the scatter function $s(\theta_1,\theta_2)$ of the object.

If the object to be imaged is one for which the first Born approximation[27] holds, then the scatter function could be obtained simply from a two-dimensional Fourier transform of the scatter potential.[28] In some of the cases examined here, volume diffraction occurs, so that there is multiple scatter and the first Born approximation is not applicable. Our approximate models will be based on this assumption of a single scatter, or kinematic regime.

4. RESULTS FOR THE MODAL METHOD

All the programs used were written in FORTRAN 77 with double precision numerical accuracy and implemented on a VAX-11/780 computer. Standard Numerical Analysis Group (NAG) routines were employed.

Two sets of data will be presented here for grooves and steps. First, plots of the variations of the intensities of the three lower diffraction orders against the grating thickness for normally incident light will be given. For normal illumination the diffraction orders are symmetric, and their phases and amplitudes are equal; therefore the

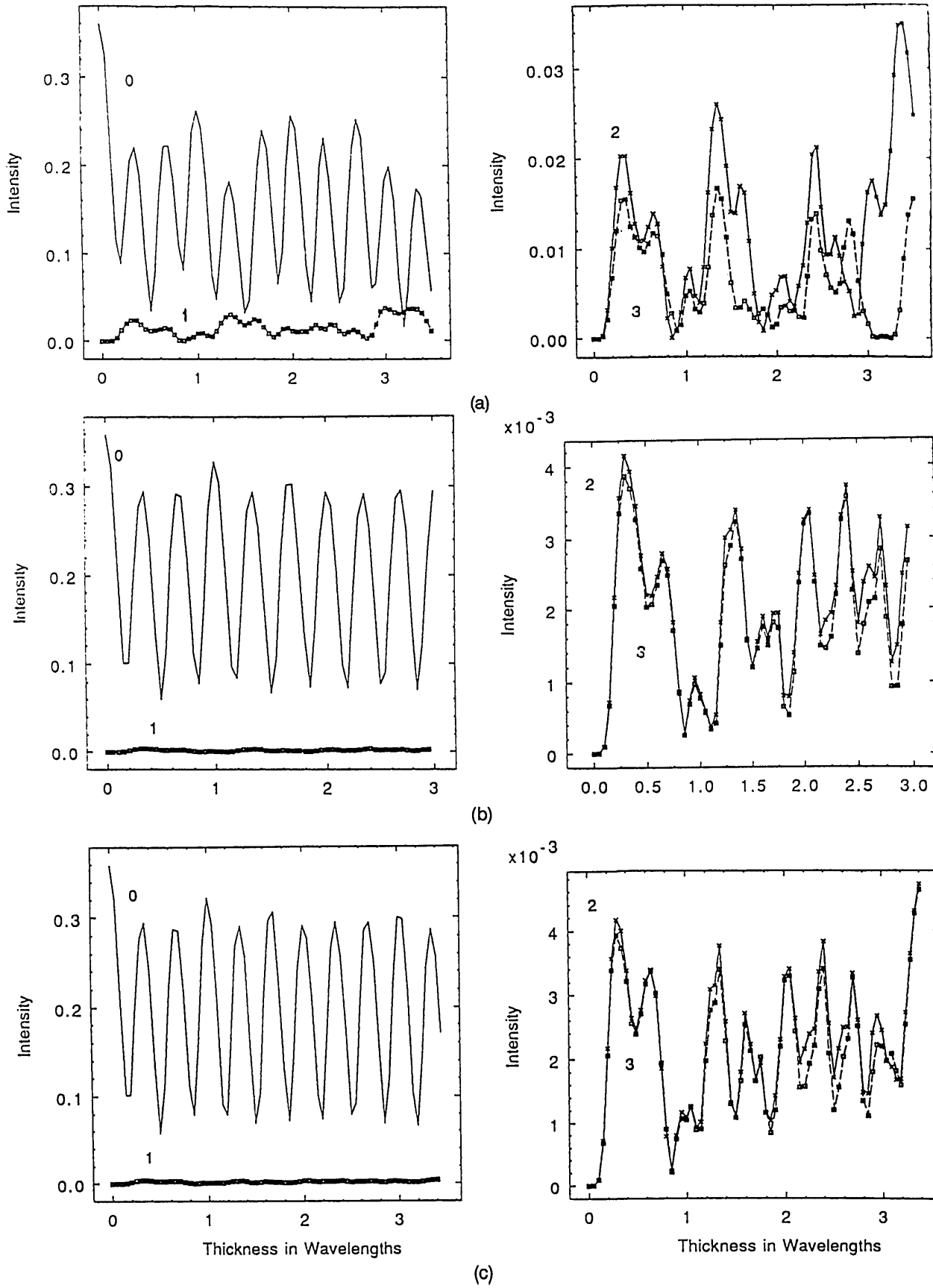

Fig. 2. (a) Variations of the zeroth through the third diffraction order intensities from an isolated G2, $n_{step} = 1.49$, groove as the thickness of the grating varies from $0 \rightarrow 4\lambda$ are shown. $W_g = 1.05\lambda$, $\Lambda = 6.1\lambda$, and $N = 11$. (b) Again a G2 groove, $W_g = 1.05\lambda$, is examined. But now the period is $\Lambda = 15.1\lambda$. The intensities of the diffraction orders decrease, and their sizes remain similar over a large range of thickness. There are positions at which the diffraction orders contain relatively little power, i.e., $T = 0.8\lambda$. In this case $N = 18$. (c) Same as in (b) but N is increased to 19 to check the convergence of the method. Changes in the results are noticeable at larger thickness for the second and third orders.

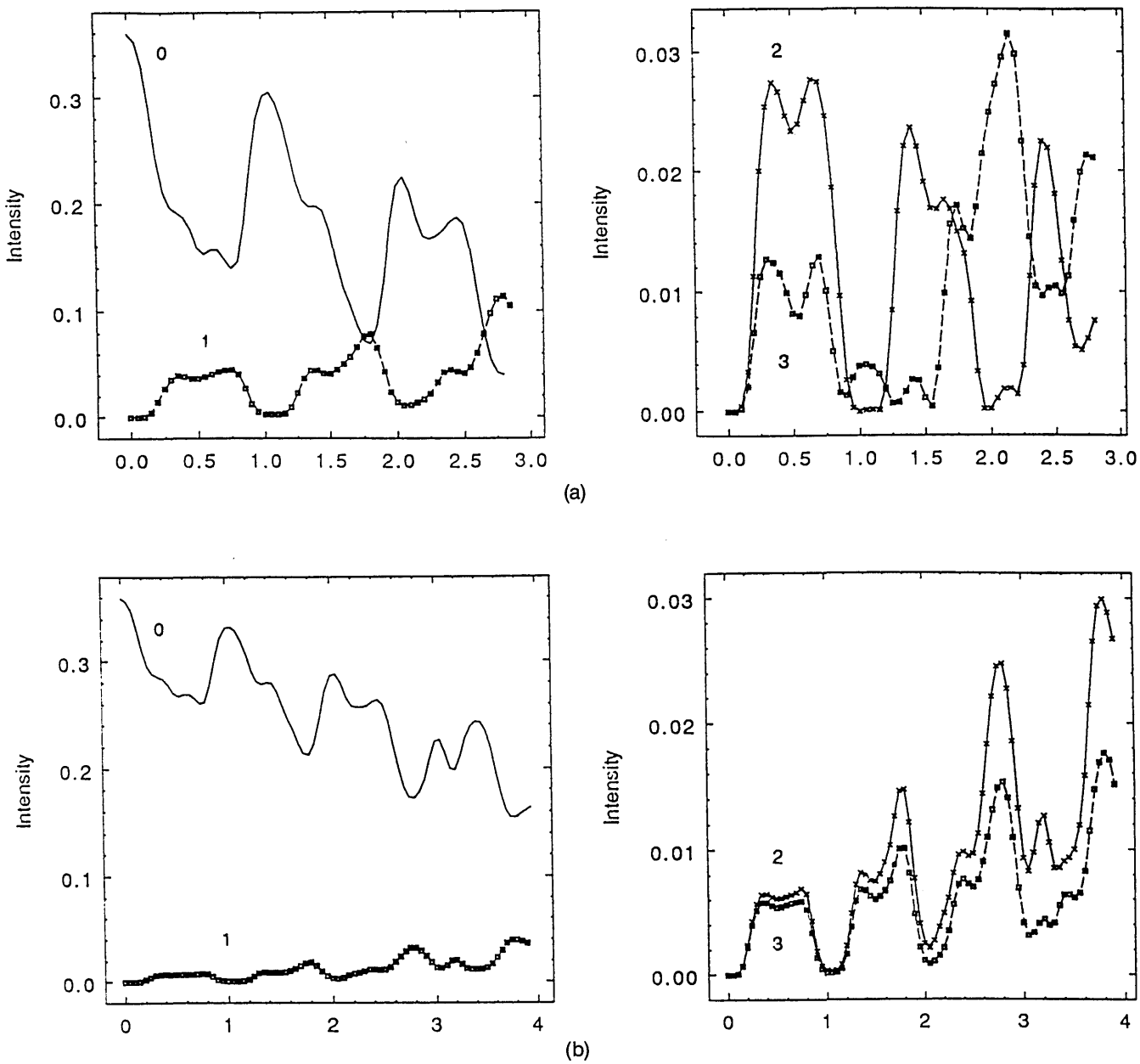

Fig. 3. The same procedure is now followed for G2 steps as was carried out for G2 grooves. Comparison of the corresponding diagrams from Figs. 2 and 3 demonstrates the effects in going from a step to a groove. (a) $W_s = 1.05\lambda$, $\Lambda = 6.1\lambda$, and $N = 11$. (b) As in Fig. 2(c), the convergence of the modal method for a larger period is checked. For an isolated G2 step, $n_{step} = 1.49$, with $W_s = 1.05\lambda$, $\Lambda = 6.1\lambda$, and $N = 19$.

positive third diffraction order is equal to the negative third order, and they are both denoted in all the figures by 3. Second, contour plots of the coherent images of the grooves and steps for normally incident light over a range of defocus positions above the top of the grating will be presented. Both sets of plots have x axes marked in wavelengths. In the image contour plots the vertical axes show the defocus position, between -10λ and $+10\lambda$, below and above the top of the grating. The contours show the intensity $I(x, z)$ levels, which are marked in five equal steps between the maximum and minimum values.

A. Examination of Diffraction Orders

As we stated in Section 1, although we want to model an isolated rectangular surface variation, we use a periodic permittivity variation. The size of the period is carefully chosen so that the effects of the scattered E fields of adjacent grooves or steps on one another are minimized. Thus the diffraction orders and the coherent images produced for several different periods and thicknesses have been examined. First, we look closely at the variations of the diffraction orders with thickness and period.

It has been found that for a separation of the edges of both types of isolated structure a period of 13λ and a step or groove 1.05λ wide the fields produced by the edges of adjacent structures do not interfere for the thicknesses and diffraction orders discussed here. Some of the general trends for G2 grooves are illustrated in Figs. 2(a) and 2(b), and for G2 steps in Figs. 3(a) and 3(b), where the intensities of the zeroth through the third diffraction orders of several structures are presented as functions of the grating thickness from 0 to 4λ. For the two forms of

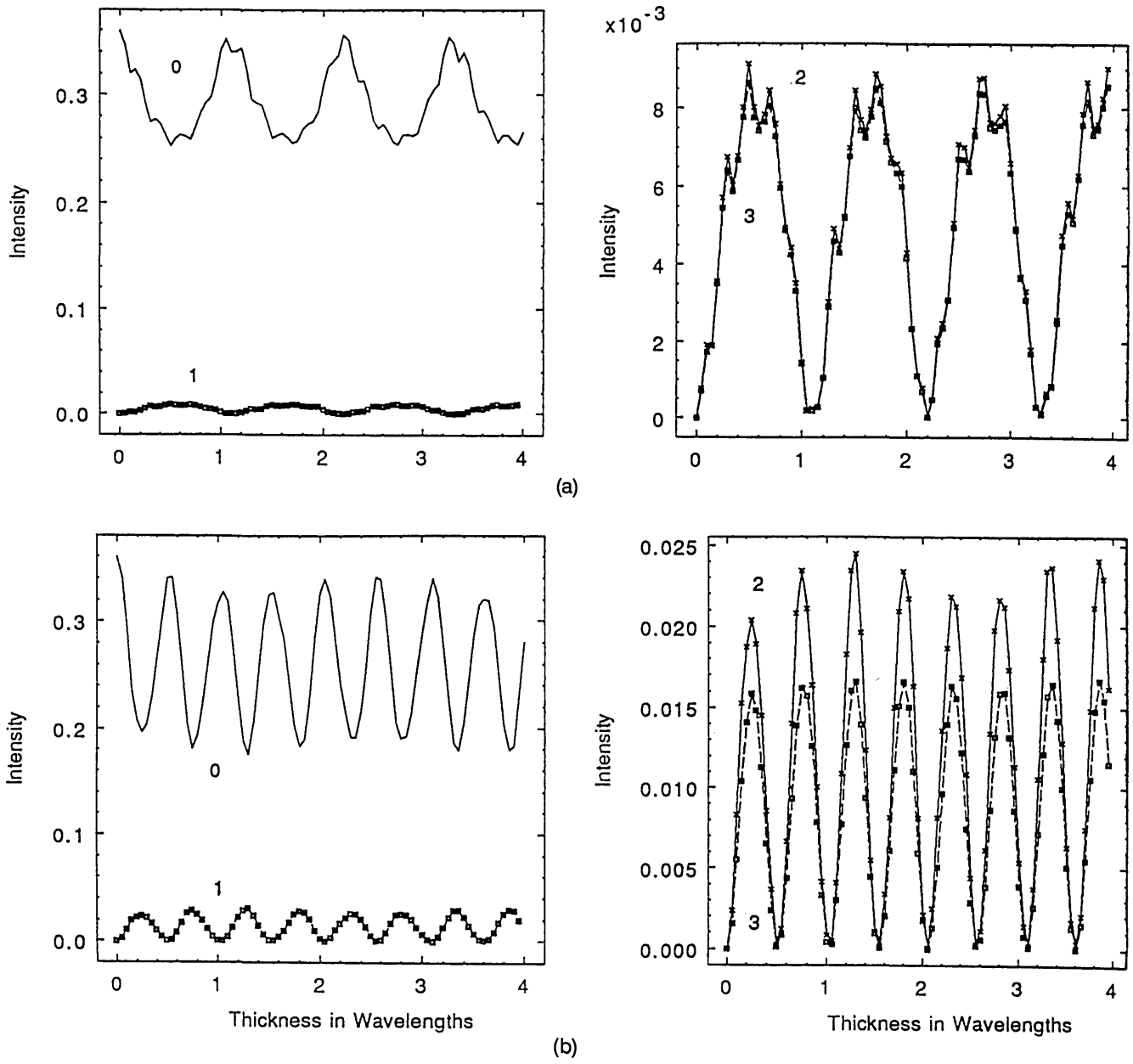

Fig. 4. Continues on facing page.

isolated structure examined, the period of the grating was allowed to increase. The results for two periods of the G2 structures, $P1 = 6.1\lambda$, and $P2 = 15.1\lambda$, are presented. There are two types of effect to note as the period increases. First, the periodic situation being modeled changes, and this change introduces some trends in the results; for example, increasing the period decreases the amount of light per period incident upon the isolated structure. Second, moving the structures away from one another will isolate them, that is, will reduce the possibility that light that has interacted with one structure will be rescattered at another. This is the first point that we wish to convey.

Let us now discuss the characteristics of these curves and try to extract some general information about the relationship between the structure and the resulting diffraction orders. For $W_g = 1.05\lambda$ in the G2 groove case (Fig. 2) the strong Fabry–Perot effect can be seen in the zeroth-order beam, owing to the large step section. This effect, it should be noted, could be used to estimate the thickness of the top dielectric layer, as intensity minima occur when the depth of the grating $T/\lambda = (2m + 1)/4n_{step} = (2m + 1)/6$, where m is an integer.

For a G2 isolated step with $W_s = 1.05\lambda$ (Fig. 3) the shapes of the variations of the diffracted orders are much more like those predicted for a square-wave grating,[12] indicating that an isolated step is much closer to that case than is an isolated groove. In particular it is interesting to note the variations of the zeroth order for the G2 step compared with the Fabry–Perot-dominated zeroth order for the G2 groove.

As the period for both structures increases, the number of beams traveling above the grating increases, and the spacings in the spatial frequencies between adjacent diffraction orders decrease. From the graphs it can be seen that, as the period increases, the predicted intensities of adjacent diffraction orders become smaller and more alike. This behavior is not unexpected, since the same central

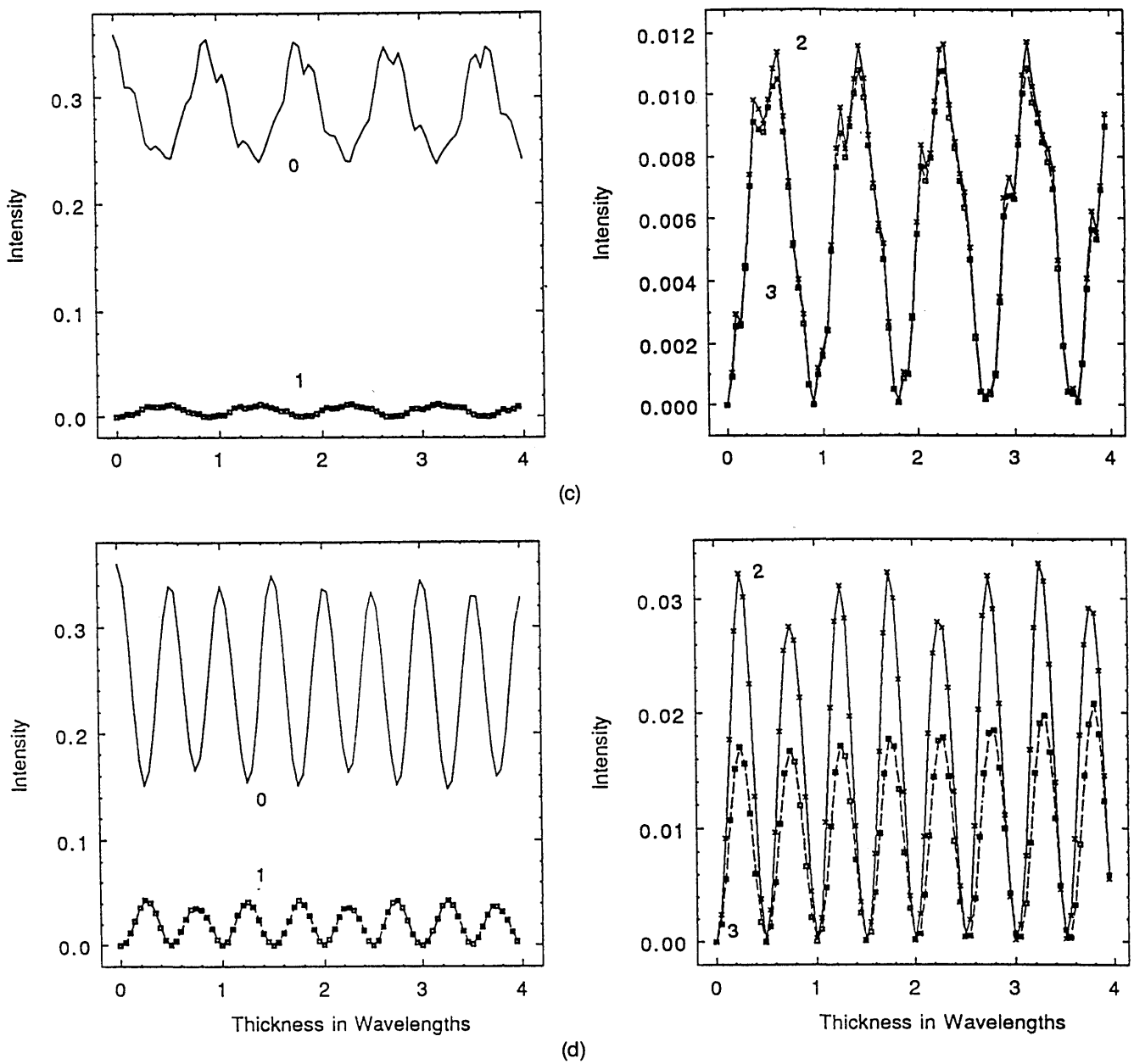

Fig. 4. (a) For a G1 groove with $W_g = 1.05\lambda$, $\Lambda = 13.1\lambda$, and $N = 17$. The diffraction-order intensities, except the zeroth, are similar in size and shape. The intensities vary slowly with thickness, indicating that volume effects, not only boundary effects, dominate the response. (b) Calculation of the response of a wider G1 groove with $W_g = 2.05\lambda$, $\Lambda = 13.1\lambda$, and $N = 17$. The shapes and sizes of the diffraction orders have altered noticeably from the results in (a). Rapid Fresnel-like interference effects can be seen for the larger width. The orders differ in size decreasing in magnitude. (c) G1 groove, $W_g = 1.05\lambda$, $\Lambda = 11.1\lambda$, and $N = 15$. (c) Along with (a), illustrates the effects of reducing the isolation of the G1 grooves. A decrease in the period strengthens the volume effect. The period of the interference with depth decreases, and the sizes of the orders increase, as does the relative difference between them. (d) For a G1 step with $W_s = 2.05\lambda$, $\Lambda = 13.1\lambda$, and $N = 17$. Convergence has been achieved in this case, and Fresnel interference effects dominate the results. The orders differ significantly in size.

structure (step or groove) is being examined, with the fifth diffraction order traveling at, for $P1 = 6\lambda$, 55 deg, for $P2 = 11\lambda$, 30 deg, and for $P3 = 15\lambda$, 19 deg. In effect similar possible end E fields are being modeled with larger numbers of beams. Structural differences mean that there is relatively more or less light reflected from the base or top of the grating to interfere above it, and the amount will affect the sizes of the beams. It can be seen that for grooves the adjacent orders are much more similar in size than for the steps; also, for the G2 steps corresponding orders are larger than for the groove case. These effects must be due in part to the amount of light reaching, and being subsequently scattered by, the sides of the groove and the fact that for the grooves the sides are submerged in the surrounding media and will be reduced in leaving the medium.

One final comment can be made about the intensity variations of the diffraction orders. The figures show that for all the structures examined there are thicknesses at which all the lower diffraction orders are small but the zeroth order is always relatively large. This implies that, although the zeroth order will always dominate any BF images, DF images will vary considerably in their light content and shapes.

The phases of the diffraction orders were also examined, as they are important to the images formed by the output beams. Because of space limitations figures will not be presented here. However, several general observations will now be made. For the G2 grooves the zeroth and the first orders are almost always approximately in phase, and the phases for the low even and odd orders appear to be consistently 180 deg out of phase. This information compliments the trends found with the intensities. For the G2 step it is found that, as the period increases, the zeroth and the first orders are π rad out of phase and the other diffraction orders tend to be in phase with the first order. These trends are in agreement with simple ideas from Fourier optics.

In summary, the following statements hold true: As the period increases for both structures, the variations of the diffraction orders (intensity and phase) with thickness decrease and becomes more regular. The sizes of the diffraction orders become smaller and the zeroth order is less disturbed by the isolated structure, as would be expected.

There are several ways of gauging the accuracy and acceptability of the numerical convergence of the diffraction orders predicted: Power conservation and reciprocity must be observed as well as the settling down of the diffraction orders, so that they vary slowly as N, the number of modes, varies. The approximation to the E field inside the grating is more theoretically sound for large N. Unfortunately, as N increases, the calculation slows, and numerical errors and overflow will occur owing to the use of large arrays and the large numbers produced by the inclusion of evanescent beams. Recent advances suggest that numerical methods do exist that avoid these problems.[29-31]

The effects of increasing N on the convergence of the results has been discussed[21] for symmetric square-wave gratings of periods larger than 10λ. For the structure discussed here it has been found that with periods 6.1λ, 11.1λ, 13.1λ, and 15.1λ, values of N of at least 11, 15, 17, and 19, respectively, must be chosen to achieve convergence for the thicknesses modeled. Thus in each case a number of evanescent waves at the top of the grating, or at the grating–air interface, are included in the approximation to the E field in the grating. These results agree well for G2 with the empirical formula proposed by Knop.[32]

The result of varying N for isolated G2 structures is illustrated in Figs. 2(b) and 2(c) for a G2 groove with $\Lambda = 15\lambda$ and $N = 18$ and 19. In Fig. 3(b) the convergent result for a G2 step with $\Lambda = 15\lambda$ and $N = 19$ is shown. Only slight intensity variations at large thicknesses occur for increased N. Power is conserved for both cases shown, but for larger N values and for larger thicknesses the higher-order beams begin to increase exponentially, and power is not conserved. This is assumed to be the best possible numerical convergence since no other substantial checks on convergence are available.

Many of the trends found for G2, $n_{step} = 1.49$, structures reappear in the G1 curves, $n_{step} = 4.0$ (Fig. 4). The plots appear greatly simplified compared with the G2 cases, as all the diffracted orders have periodic zeros except the zeroth. This happens because there is no mismatch between the substrate and the layer containing the step or the groove, and therefore multiple reflections are absent. In the G1 case, scatter that is due to the step is stronger than in the G2 case, as the steps are made of material with a higher refractive index. Therefore stronger volume effects, which are due to multiple scatter, are not hidden, as in the G2 case, by the step slabs acting as Fabry–Perot étalons.

It is found that for an isolated G1 structure $n_{step} = 4.0$, convergence is much harder to ensure than for the equivalent G2 case. The high refractive index creates numerical difficulties for small structure widths. This problem arises from the slow convergence of the Fourier series expansion of the structure's permittivity cross section and the numerical difficulties that come from working with big complex arrays. The numerical limitations on the convergence for the G1 isolated step forced us to examine structures that are wider than one wavelength. Some results that we believe are satisfactory are presented in Fig. 4(d).

For the G1 grooves with $W_g = 1.05\lambda$ there are strong scatter effects that dominate any simple interference that is due to reflections from the shifted surface. Plots are therefore included for larger groove and step sizes $W_g = W_s = 2.05\lambda$ in Figs. 4(b) and 4(d). The resulting zeroth order for grooves is less oscillatory than for the corresponding steps, as light is rescattered within the embedded groove and surrounding material as it tries to leave the grating.

For the G1 step [Fig. 4(d)] the intensities are as in the G2 step case [Figs. 3(a) and 3(b)] larger and differ more from one another compared with orders in the groove case. It is also found that the phases of the higher diffraction orders are similar. For the isolated G1 groove the intensities are smaller than for the step, and the phases of adjacent diffraction orders are found to be π rad out of phase. As before these results are in agreement with simple physical ideas.

B. Examination of Coherent Images

The previous results are now applied as we examine the coherent BF and DF images of the G1 and G2 structures. Calculations for DF images are carried out without the inclusion of the zeroth order. The resulting images thus lose their bright background as the large zeroth order, which can dominate and swamp finer detail, is filtered out. BF and DF images of the same structure, in varying steps of grating thickness, for isolated steps and grooves of different widths and periods were examined for different N.A.'s and for different numbers of modes, N, included for convergence. The results are presented as contours of intensity, isophotes, plotted as a function of the x scanned position over one period, and the z defocus position, $\pm 10\lambda$ above and below the top of the structure. All steps are centered at the $x = 0.0$ position. The contour form has been chosen because it permits a great deal of information to be concisely presented, although the format runs the risk of some ambiguity because of the limit on the number of contours that can be clearly marked.

Only a small number of the graphs produced will be presented here to show the trends of the variations of the images. The convergence of the modal method for a set of physical parameters has already been investigated. The BF and DF images of steps and grooves of similar dimensions are now examined. First the fact that the objects are isolated from one another can be investigated by examining some images. In focus there are intensity variations between the isolated G2 groove structures in both

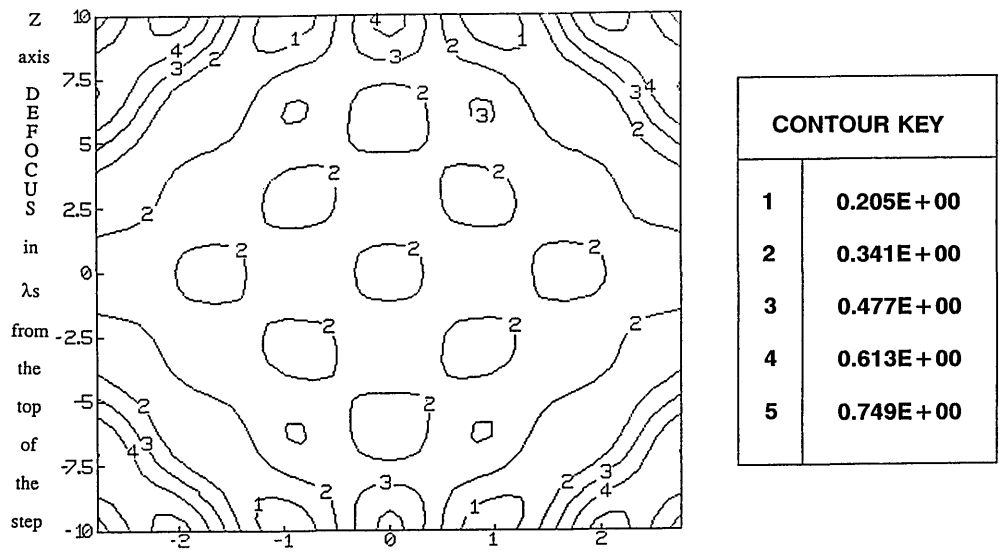

Fig. 5. Coherent BF image of a G2, $n_{step} = 1.49$, groove structure with $W_g = 1.05\lambda$, centered halfway between two isolated grooves. $\Lambda = 11.1\lambda$, $T = 1.0\lambda$, $N = 15$, and the N.A. is 6/11. (The +6 to −6 diffraction orders are included in the image.) Although there are maxima above and below the structure, no image appears at $x = 0$, far from both grooves.

the BF image (Fig. 5) and the DF image; however, these are small interference fringes. Large maxima do appear out of focus above and below the midpoint between the grooves. Note that, because of the periodic nature of the structure being modeled, self-imaging, the so-called Talbot effect,[33] will occur in the field above the grating and that this effect does occur here.

BF images [Figs. 6(a) and 6(c)] and DF images [Figs. 6(b) and 6(d)] for various thicknesses of the G2 isolated groove indicate that little accurate information can be obtained from the BF image contour plots on their own. There is, for example, a large variation of the BF image with thickness for a G2 groove, and often the positions of the edges in the BF image seem to be 2λ apart, for a λ-wide structure. The positions of the top and bottom of the grooves are also indistinct. However, the corresponding DF image plots give more-accurate information about the width of these structures. It is interesting to see how these results are clearly related to the beam intensities shown in Fig. 2.

From the graphs it seems clear that pooling and combining the sets of information for a particular grating contained in the BF and DF image contour plots of intensity variation with defocus has some advantages. From the DF image definite width information can be extracted. As has been stated, it is possible to estimate the depth of the structure by calculating the relative phase of the zeroth order. For a G2 structure the procedure is relatively simple: examination of the zeroth diffraction order provides a prediction of the grating thickness with the Fabry–Perot characteristics of the step, or top layer, into which the groove is etched.

The position and size of the defocused intensity maxima also give some information as to the position and size of isolated structures. For example, for most thicknesses that were examined the maximum intensity of the light for a BF image in the range of defocus examined was below the top of the grating, although it could be above the top [Fig. 6(a)]. The intensity maxima in the DF images are always found to lie below the top of the grating, where the groove is located. In the DF image case, the x positions of the edges are more clearly defined, and the variations in the z direction are more distinct as the groove becomes deeper. The location of the maximum drops farther below the x axis as the G2 groove becomes deeper.

The results when the width of an isolated G2, $n_{step} = 1.49$, groove increases compared with the wavelength of the incident radiation is illustrated in Fig. 7. Four distinct maxima appear in the DF image contour plots. These maxima correspond to the top, bottom, and sides of the structure. As the isolated structure's width increases (the period also increasing so as to maintain separation) the maxima decrease in intensity but increase in extent and separation [Fig. 7(d)]. The two side edges stay well defined in the DF image, the positioning in the x direction being still good. However, the top and bottom intensity maxima become detached and float away above and below the groove.

Next the BF and DF images for isolated G2 steps, $n_{step} = 4.0$, presented in Fig. 8, are examined. In the DF images it can be seen that for thicknesses $T = (2m + 1)\lambda/2$ [Fig. 8(c)], where m is an integer, there is a single maximum. For $T = m\lambda$, Fig. 8(b), four maxima appear, one at each edge, or side, of the object. As a general rule it seems that the BF image [Fig. 8(a)] is not of much practical metrological use in these situations. Smaller intensity values appear in the DF image contour plots for $T = m\lambda$, as expected from the diffraction-orders-versus-thickness plots previously calculated [Figs. 3(a) and 3(b)]. Thus two distinct DF image regimes appear to exist for isolated steps, analogous to the two regimes for square-wave gratings.[12] This effect has not been found to occur for isolated grooves (Fig. 6).

We now examine the images of isolated G1, $n_{step} = 4.0$, grooves. First, we investigate the general effects of varying the numerical aperture of the imaging system. The DF image contour plot of a small surface variation, less

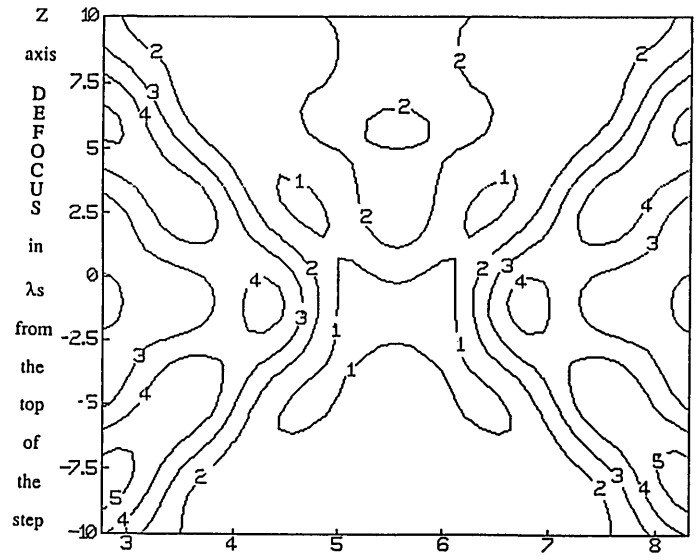

CONTOUR KEY	
1	0.536E-01
2	0.160E+00
3	0.266E+00
4	0.372E+00
5	0.478E+00

(a)

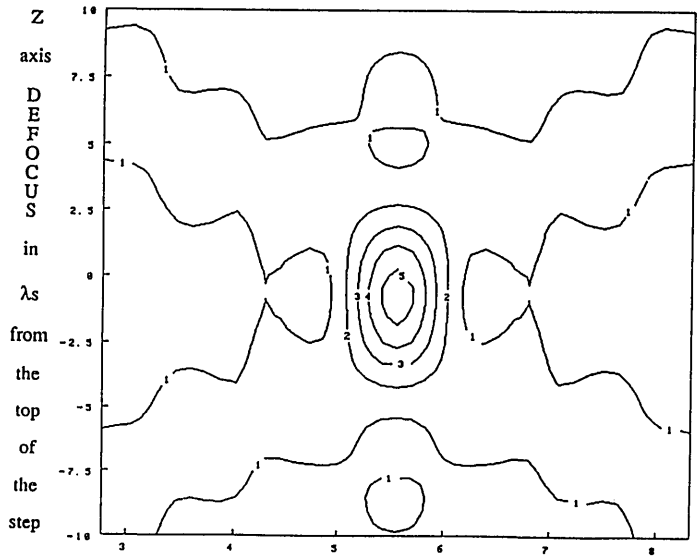

CONTOUR KEY	
1	0.337E-01
2	0.101E+00
3	0.168E+00
4	0.236E+00
5	0.303E+00

(b)

Fig. 6. Continues on facing page.

than one wavelength in the x and z dimensions, reveals an image analogous to that which would be expected to be produced by a point object. The intensities are small, as would be expected. The result is similar to the product of two orthogonal sinc functions, one in the defocus, or z direction, the other in the x direction. Two ridges can be seen crisscrossing the plot like an X centered on the intensity maximum. The angles at which the ridges lie are defined by the N.A. of the imaging system, which also defines the resolution of the system. The effects of a larger N.A. can be demonstrated by a graph in which an increased number of diffraction orders are included in the image calculated.

To demonstrate the effect that changing the N.A. has on the DF image of a G1 isolated groove of depth 0.5λ and width $W_g = 0.5\lambda$, a period of 11.1λ is used. Figure 9(a) shows an image with $\alpha = 35$ deg (containing all the orders -6 to $+6$), and Fig. 9(b) has $\alpha = 50$ deg (-8 to $+8$). It is also interesting to note that for this narrow groove, as the thickness is increased, most of the scatter still appears to take place at the top surface or the mouth of the groove. In fact, although the intensity of the contours changes, the shape and position do not alter for a wide range of groove depths. Thus a cutoff effect similar to that which occurs in the case of a waveguide takes place.

For a G1 groove of width $W_g = 1.05\lambda$ the thickness T is varied, and the resulting BF and DF images are shown in Fig. 10. Unlike in the G2 step case, for $T = m\lambda$ the DF image does not have four maxima, only one; however, it does contain less light than the $T = (2m + 1)\lambda/2$ cases. The DF image intensity maximum never appears above the axis; however, the BF image varies considerably as the thickness changes. In this case the BF image does seem to be useful, as the ridges crossing the contour plot

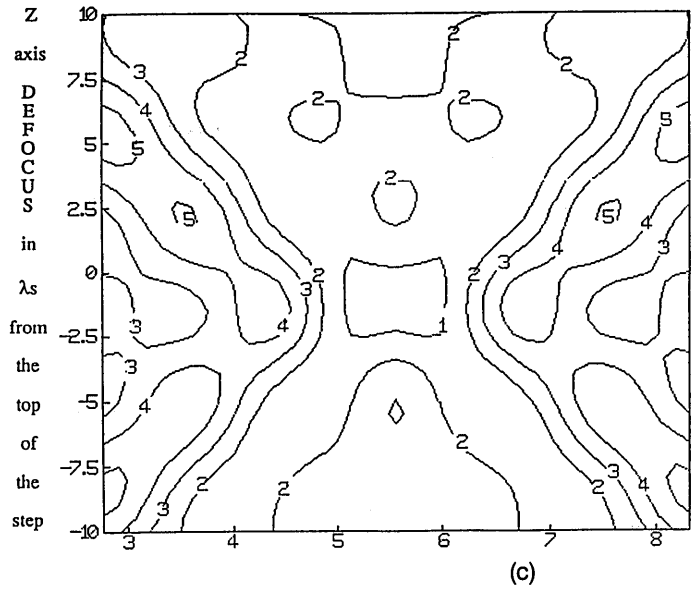

(c)

CONTOUR KEY	
1	0.527E-01
2	0.156E+00
3	0.260E+00
4	0.364E+00
5	0.468E+00

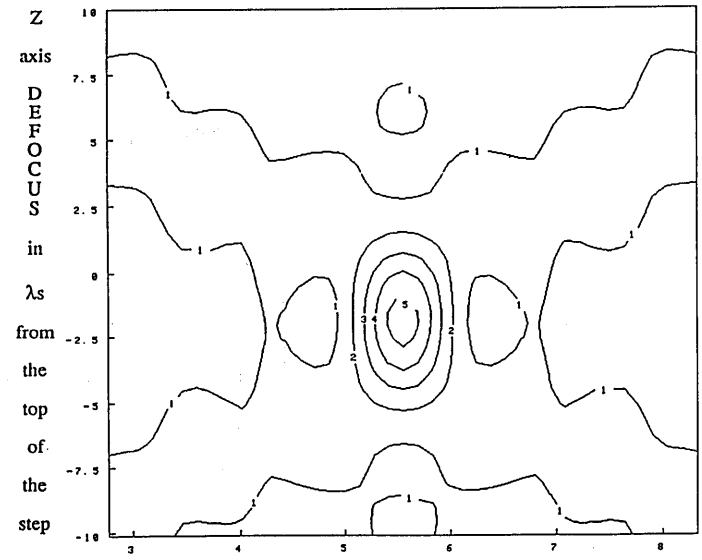

(d)

CONTOUR KEY	
1	0.268E-01
2	0.802E-01
3	0.134E+00
4	0.187E+00
5	0.241E+00

Fig. 6. (a), (b) BF and DF images of a G2 groove $W_g = 1.95\lambda$ with $T = 0.75\lambda$, $\Lambda = 11.1\lambda$, $N = 15$, and the N.A. is 6/11. The groove is centered at $x = 5.55\lambda$. (c), (d) BF and DF images of a G2 groove $W_g = 1.05\lambda$. Again $\Lambda = 11.1\lambda$, $N = 15$, and the N.A. is 6/11. But in these cases, $T = 1.75\lambda$, i.e., the base of the groove is at -1.75λ on the z defocus axis.

are centered at the $z = 0$ axis, especially when $T = m\lambda$. In the DF images the groove edges are well defined. The defocus intensity maximum corresponding to the structure consistently lies below the top of the grating and appears to move downward as the thickness of the structure increases. Therefore for this structure a series of gradually defocused DF images may be sufficient for determination of both the width and the thickness of the structure.

The Zernike phase contrast method[27] can be used with weakly scattering objects, for example, dielectric gratings less than $\lambda/4$ in thickness. The zeroth order is shifted by $\pi/2$ rad with respect to the other orders, and then more-accurate information can be extracted about the structure. Several other similar techniques based on the Schlieren method[27] are also available to deal with thin phase objects, and the limitations of the techniques can be analyzed by the methods described here.

5. APPROXIMATE MODELS

Two approximate models that are currently being investigated will now be proposed, and a short introduction will be made.

Model 1

In the first model the response of the scatterer is assumed to be that of an isolated point or line scatterer (see Fig. 11), that is, the scattering function is defined as $s(\theta_1, \theta_2) = 1.0$. The image of such an object can be calculated with the optical coordinates u and v,[27]

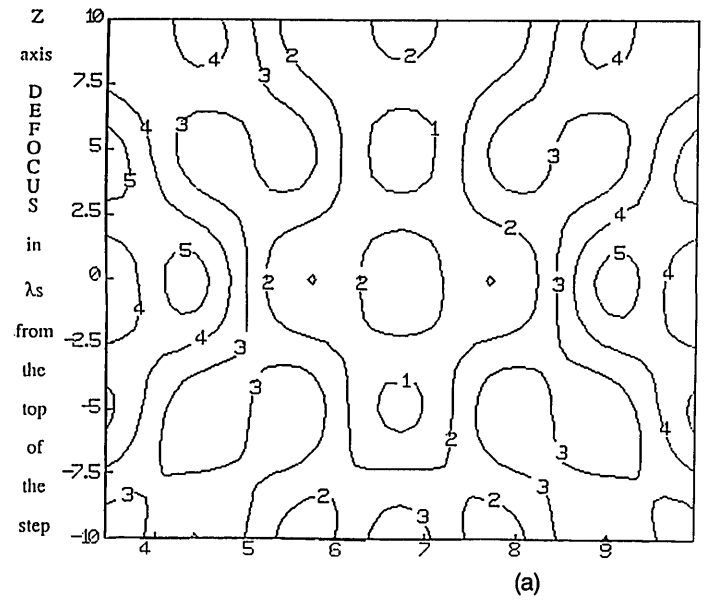

CONTOUR KEY	
1	0.143E+00
2	0.218E+00
3	0.292E+00
4	0.367E+00
5	0.442E+00

(a)

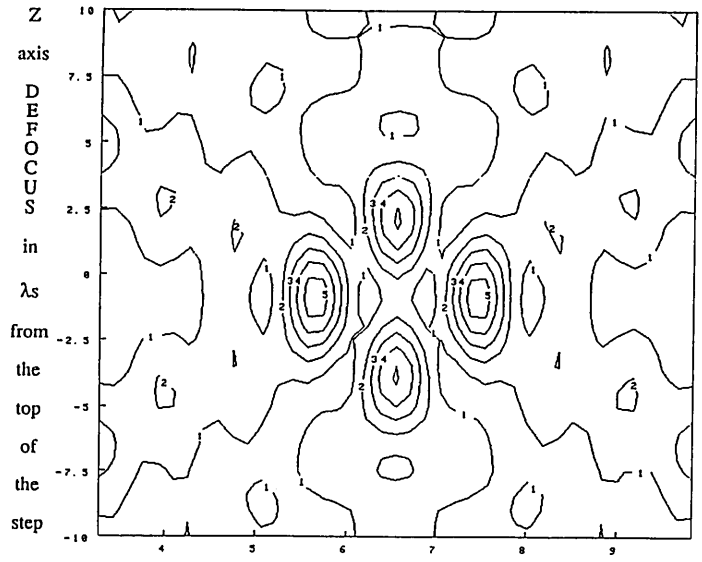

CONTOUR KEY	
1	0.157E-01
2	0.472E-01
3	0.787E-01
4	0.110E+00
5	0.142E+00

X axis, scanned direction, marked in wavelengths: 0 at center of step

(b)

Fig. 7. Continues on facing page.

$$u = kz\,\sin^2(\alpha) \quad \text{or} \quad u = 4kz\,\sin^2(\alpha/2); \qquad v = kx\,\sin(\alpha), \tag{7}$$

where α is the objective imaging aperture and the second form of u gives better agreement for large N.A.'s.[34]

Substitution of a variable X, defined as

$$X = \frac{\sin\theta_2}{\sin\alpha}, \tag{8}$$

into Eq. (6) with the second form of u in Eqs. (7) gives

$$I(u,v) = \left|\int_0^1 \cos(vX)\exp\left(\frac{1}{2}juX^2\right)\mathrm{d}X\right|^2. \tag{9}$$

This integral can be rewritten in terms of the Fresnel integrals, $C(x)$ and $S(x)$, or the error function, $\mathrm{Erf}(x)$.[35] The methodology can be extended to allow for reflections from the dielectric substrate, as shown in Figs. 12(a) and 12(b), and can be used to calculate the positions of edges for wider structures [Fig. 12(c)] and isolated grooves [Fig. 12(d)]. In this case

$$I_s(u,v) = \left|\int_0^1 \cos(vX)\exp\left(\frac{1}{2}ju_1X^2\right)\mathrm{d}X + \int_0^1 R(\theta_2)\cos(vX)\exp\left(\frac{1}{2}ju_2X^2\right)\mathrm{d}X\right|, \tag{10}$$

where $R(\theta_2)$ is the amplitude of the light reflected from the surface as a function of the angle of incidence and u_1

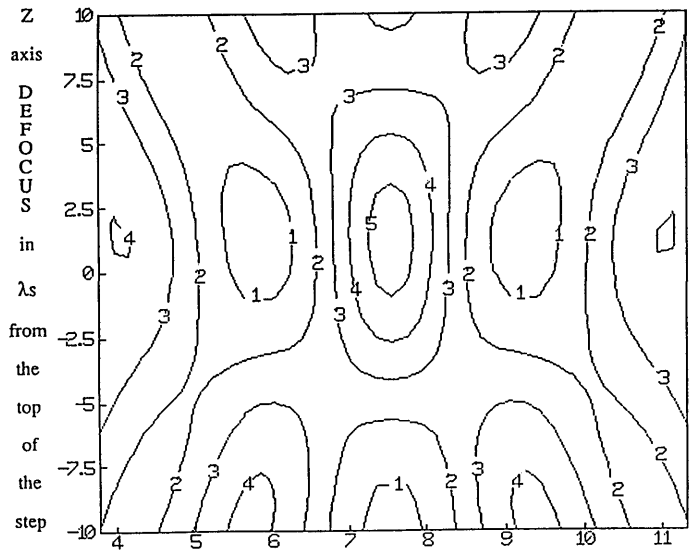

(c)

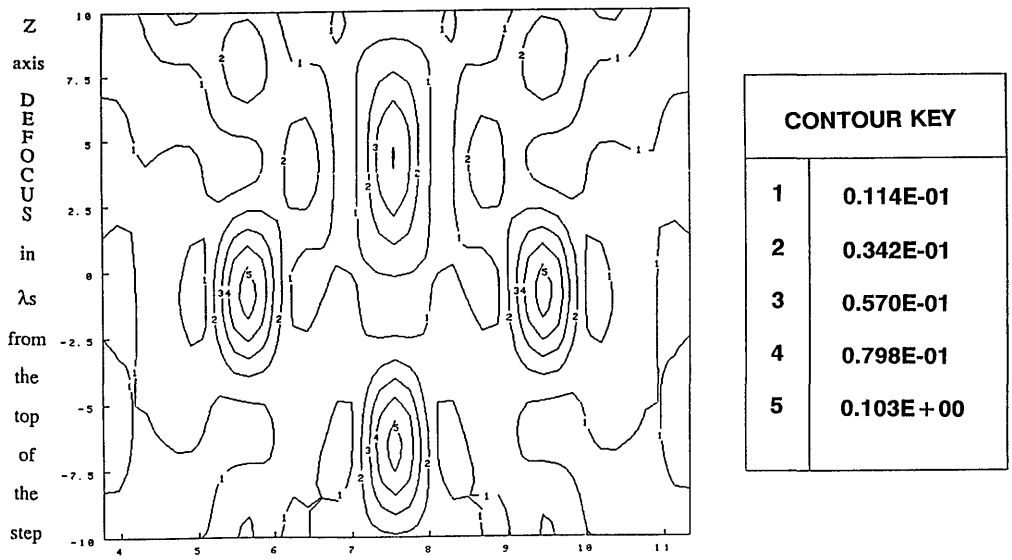

(d)

Fig. 7. (a), (b) BF and DF images of a G2 isolated groove with $W_g = 2.05\lambda$, $T = 1.0\lambda$, $\Lambda = 11.1\lambda$, $N = 17$, and the N.A. = 8/11. (c), (d) BF and DF images of a G2 isolated groove with $W_g = 4.05\lambda$, $T = 1.0\lambda$, $\Lambda = 15.1\lambda$, $N = 19$ and the N.A. = 8/15. The edges of the groove are farther apart than in (a) and (b). The N.A., and thus resolution of the images, has decreased.

and u_2 allow for the different defocus positions of the two lines.[36] Essentially a real amplitude and its shifted reflection are added together.

Model 2

It is also possible to model diffraction by the structure with a two-dimensional Fourier transform of a rectangular function (Fig. 13). First, however, it must be shown that this can be simply related to the scattering function of the isolated structure. We combined the work and notation of Wolf[28] and Sheppard[37] to calculate an integral expression for the image of the scatterer. The amplitude scattering function of a weakly scattering object in a monochromatic system is given by

$$s(\theta_1,\theta_2) = \int_{-\infty}^{+\infty}\int_{-\infty}^{+\infty} t(x,z)\exp\{jk[(\sin\theta_1 + \sin\theta_2)x + (\cos\theta_1 + \cos\theta_2)z]\}dxdz, \quad (11)$$

where $t(x, z)$ is the complex scattering amplitude of the object.

The spatial frequency spectrum of the object can be written as

$$T(m,r) = \int_{-\infty}^{+\infty}\int_{-\infty}^{+\infty} t(x,z)\exp[2\pi j(mx + rz)]dxdz, \quad (12)$$

where, when $\theta_1 = 0$, for normal incidence,

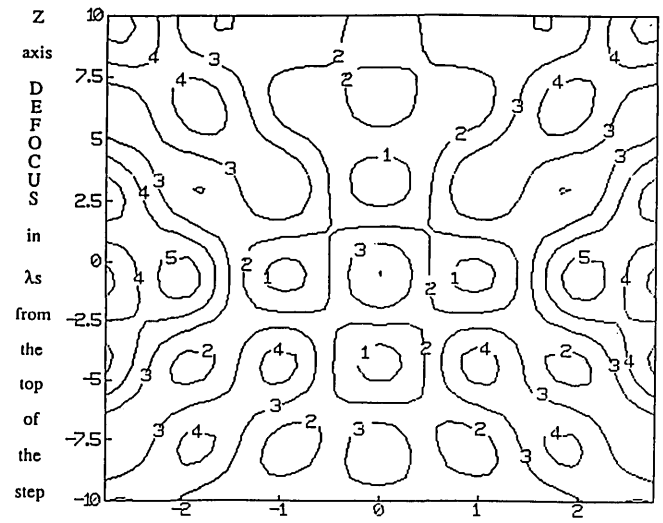

CONTOUR KEY	
1	0.146E+00
2	0.226E+00
3	0.306E+00
4	0.386E+00
5	0.466E+00

(a)

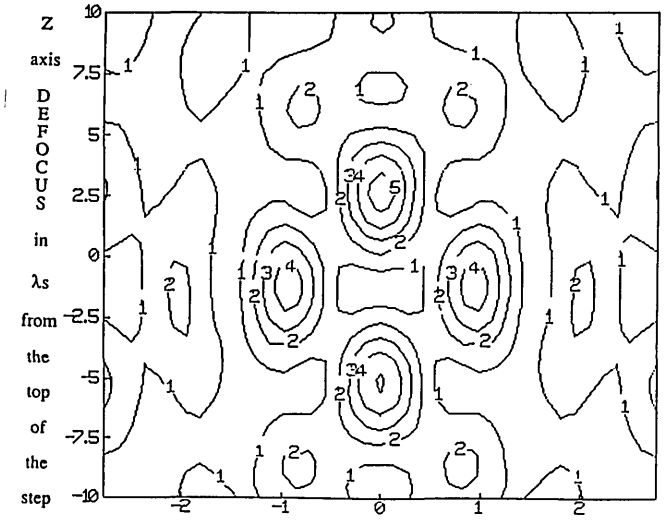

CONTOUR KEY	
1	0.655E-02
2	0.196E-01
3	0.326E-01
4	0.457E-01
5	0.587E-01

(b)

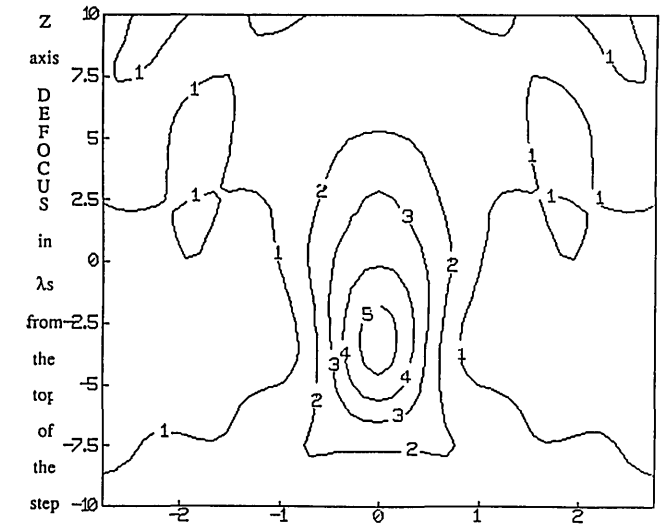

CONTOUR KEY	
1	0.682E-01
2	0.201E+00
3	0.335E+00
4	0.468E+00
5	0.601E+00

X axis, scanned direction, marked in wavelengths: 0 at center of step

(c)

Fig. 8. (a), (b) BF and DF images of a G2 step. $W_s = 1.05\lambda$, $\Lambda = 11.1\lambda$, $N = 15$, $T = 1.05\lambda$, and the N.A. = 6/11. The orders for this case are examined in Fig. 3(b). The BF image contains little accessible information. The DF image contains very little light, but the intensity maxima clearly indicate the position of the step. (c) DF image of a G2 step. $W_s = 1.05\lambda$, $L = 11.1\lambda$, $N = 15$, $T = 1.5\lambda$, and the N.A. = 6/11. There is only one maximum, and the position of the step is less clear.

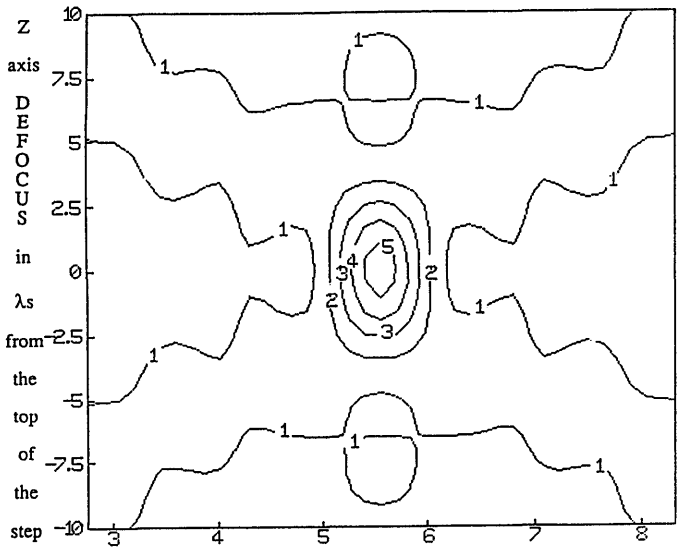

CONTOUR KEY	
1	0.275E+01
2	0.825E-01
3	0.138E+00
4	0.193E+00
5	0.248E+00

(a)

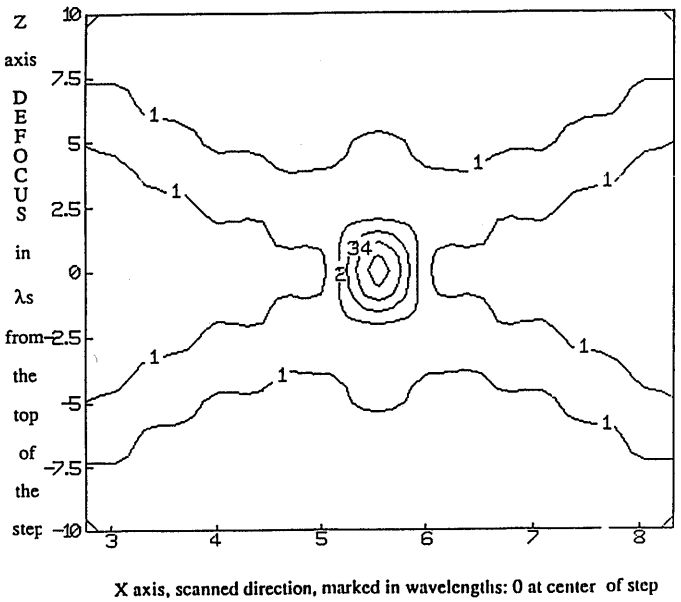

CONTOUR KEY	
1	0.448E-01
2	0.134E+00
3	0.224E+00
4	0.313E+00
5	0.403E+00

X axis, scanned direction, marked in wavelengths: 0 at center of step

(b)

Fig. 9. (a) DF image of a G1 isolated groove, $W_g = 0.5\lambda$, $L = 11.1\lambda$, $N = 15$, $T = 0.5\lambda$, and the N.A. = 6/11. Such an object acts as a point source or line object. (b) DF image of the same structure as examined in (a); however, in this case the N.A. is increased to 8/11. There is a decrease in the slopes of the crossing ridges and a marked improvement in resolution.

$$m = \frac{\sin(\theta_2)}{\lambda}; \qquad r = \frac{1 - \cos(\theta_2)}{\lambda}, \tag{13.1}$$

$$(\lambda m)^2 + (\lambda r)^2 = 2\lambda r. \tag{13.2}$$

For the imaging geometry used, these parameters will vary within the following limits (Fig. 14):

$$-\sin(\alpha) \le \lambda m \le \sin(\alpha); \qquad 1 - \cos(\alpha) \le \lambda r \le 2. \tag{14}$$

Previously it has been indicated[38,39] that with the Kirchhoff approximation and the assumption of TE polarized incident light, the two-dimensional surface scatter function can be related to the two-dimensional Fourier transform of the surface profile as follows:

$$s(\theta_1, \theta_2) = \left[\frac{(\lambda m)^2 + (\lambda r)^2}{2\lambda r}\right] T(m, r). \tag{15}$$

For the conventional coherent case examined here Eq. (13.2), with the assumption that $t(x, z)$ is separable into $t(x)t(z)$, leads to

$$s(0, \theta_2) = T(m)T(r) = T(m, r). \tag{16}$$

Thus the scattering function and the spectrum are closely

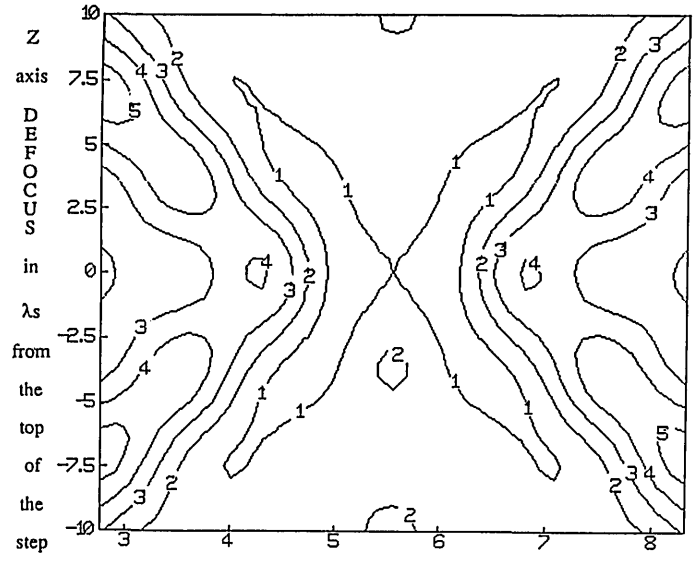

(a)

CONTOUR KEY	
1	0.759E-01
2	0.227E+00
3	0.379E+00
4	0.530E+00
5	0.682E+00

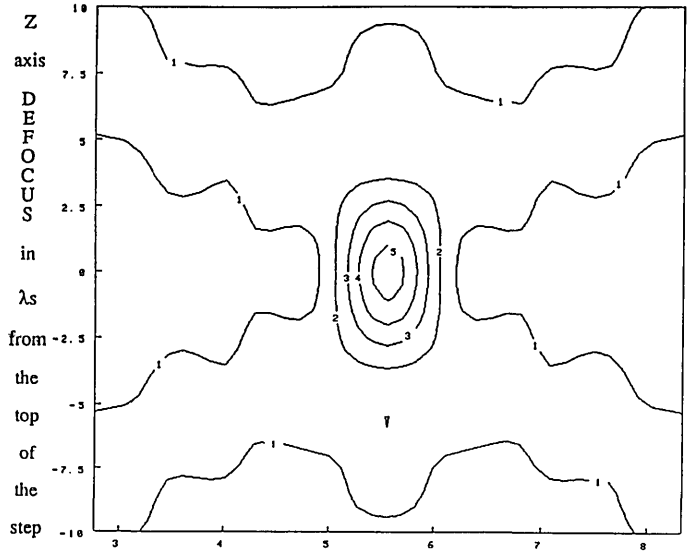

X axis, scanned direction, marked in wavelengths: 0 at center of step

(b)

CONTOUR KEY	
1	0.639E-01
2	0.192E+00
3	0.320E+00
4	0.448E+00
5	0.575E+00

Fig. 10. Continues on facing page.

related, and this definition can now be used in conjunction with Eq. (6).

We now turn to the theory and notation of Wolf[28] and work in the first Born approximation. We start with the scalar wave equation

$$\nabla^2 U(x,z) + k_0^2 n^2(x,z) U(x,z) = 0, \tag{17}$$

and assume it is slightly perturbed

$$U(x,z) = U^i(x,z) + U^s(x,z). \tag{18}$$

Substitution of Eq. (18) into Eq. (17) yields:

$$(\nabla^2 + k_0^2) U^s(x,z) = F(x,z) U(x,z) = -k^2[n^2(x,z) - 1] U(x,z), \tag{19}$$

where $F(x,z)$ is the scattering potential of the object and can be written in our case as

$$F(x,z) = -k_0^2(\epsilon_s - \epsilon_a)\mathrm{rect}\left(\frac{x}{a}, \frac{z}{b}\right), \tag{20}$$

where a and b are the width and height respectively of the isolated step structure. The two-dimensional Fourier transform or spectrum of $F(x,z)$ is given by

$$\hat{F}(u,w) = -k_0^2 \hat{\epsilon} ab \ \mathrm{sinc}\{au, bw\}, \tag{21}$$

where u and w are the spatial frequencies along the x and z axes and $\hat{\epsilon}$ is the permittivity difference [from Eq. (20)].

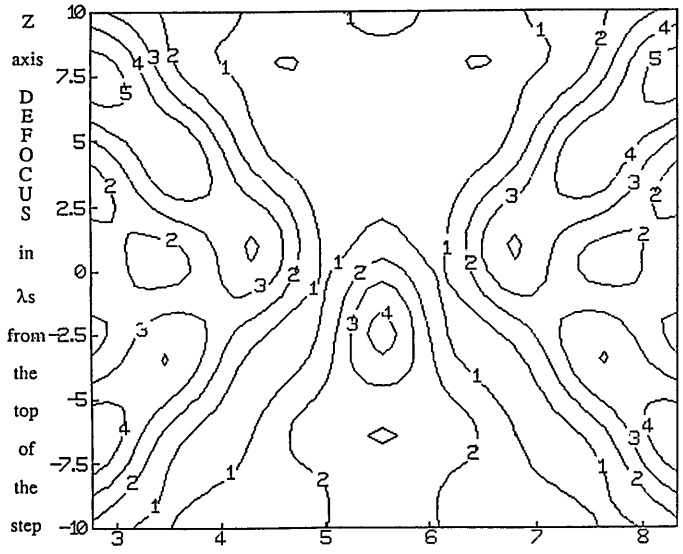

CONTOUR KEY	
1	0.100E+00
2	0.299E+00
3	0.498E+00
4	0.697E+00
5	0.895E+00

(c)

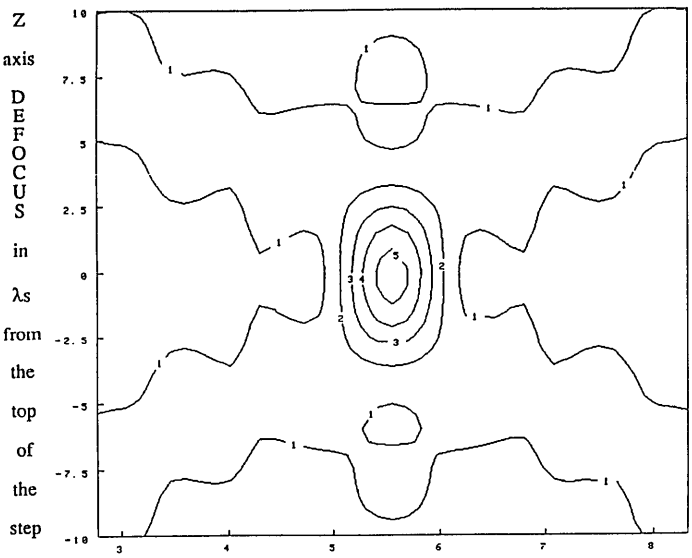

CONTOUR KEY	
1	0.106E+00
2	0.317E+00
3	0.528E+00
4	0.739E+00
5	0.951E+00

X axis, scanned direction, marked in wavelengths: 0 at center of step

(d)

Fig. 10. (a), (b) BF and DF images of a G1 groove, $W_g = 1.05\lambda$. $\Lambda = 11.1\lambda$, $N = 15$, $T = 1.0\lambda$, and N.A. = 6/11. In the BF image the ridges cross at $z = 0$, the top of the structure. (c), (d) BF and DF images for a deeper G1 groove, $W_g = 1.05\lambda$. In this case $\Lambda = 11.1\lambda$, $T = 1.5\lambda$, and N.A. = 6/11. The base of the groove is physically at -1.5λ in the z defocus direction.

The scattered field can be written as

$$U^s(x,z) = \iint A^{(-)}(p;0)\exp[jk_0(px - mz)]\mathrm{d}m\mathrm{d}p, \quad (22)$$

where the A is the spectral amplitude function

$$A^{(-)}(p;0) = -j\frac{k_0}{8\pi^2 m}\iint F(x,z)\exp\{-jk_0[px - (m-1)z]\}\mathrm{d}x\mathrm{d}z. \quad (23)$$

This expression is related to the two-dimensional Fourier transform of the scattering potential, and therefore the intensity of the scattered field in the reflection direction

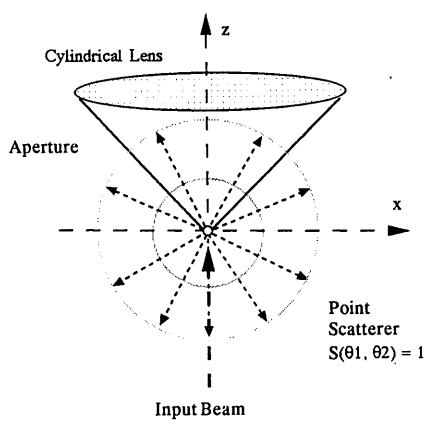

Fig. 11. Transmission geometry imaging; reflection geometry imaging is examined in the paper. The point scatterer scatters weakly and symmetrically in all directions. No skew waves are involved as a cylindrical imaging system is used.

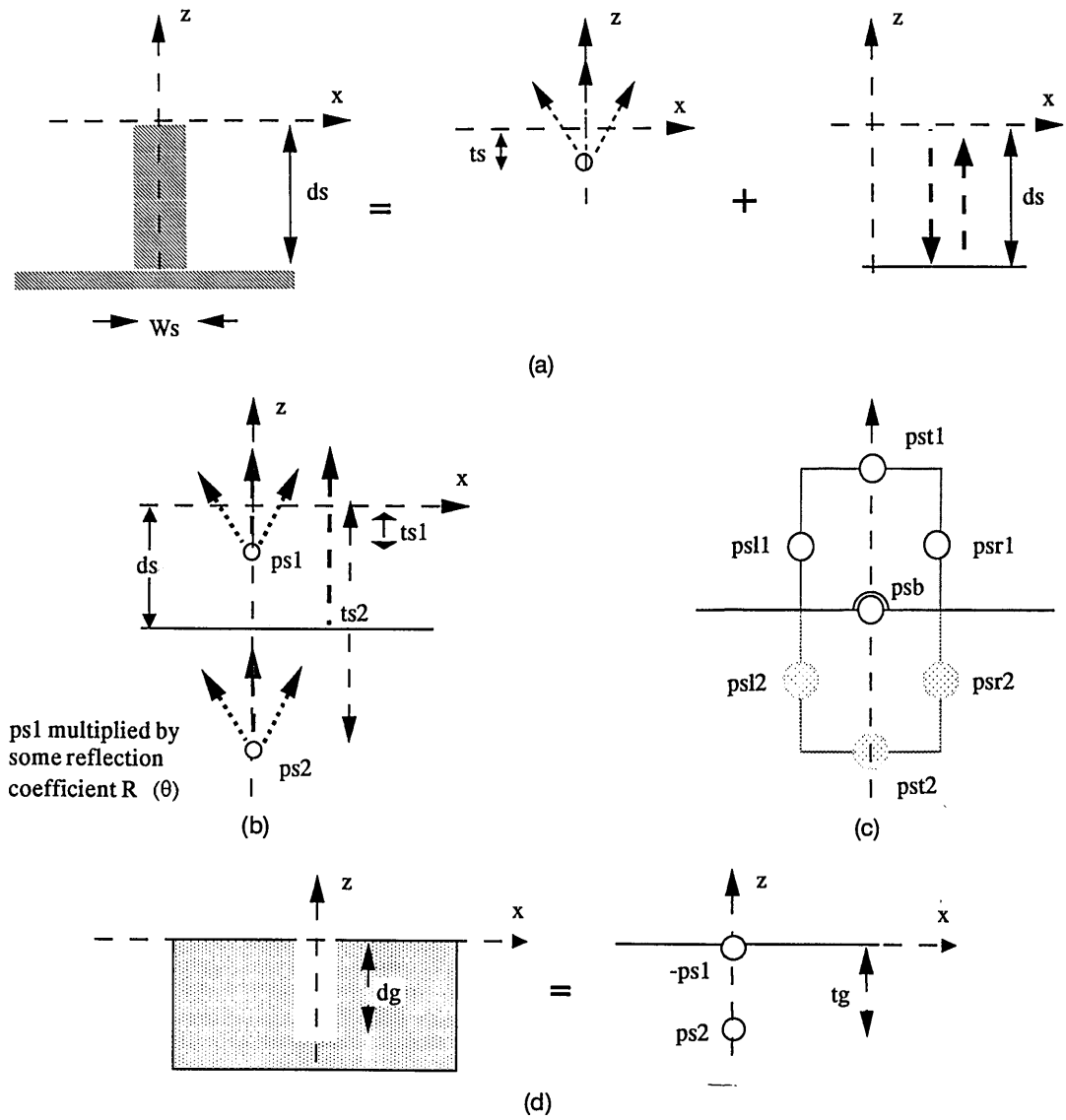

Fig. 12. (a) Diffracted light from a weakly scattering isolated step, made of the same material as the substrate, modeled by the light diffracted by a defocused point scatterer, $z = ts$, plus the large reflection from the substrate (Model S1.1). The point scatterer (ps) may not be positioned at the depth of the edge it represents, to produce optimum agreement. (b) In Model S1.2 the reflections from the surface of the substrate of the downward-traveling light from ps1, giving ps2, interfere with the upward traveling light from ps1 and the substrate. Allowance can be made for the matched condition at the bottom of the step if the width is larger. The defocus positions of the effective point scatters, ts1 and ts2, must be included. (c) Model S1.3 could be used for wider steps. The edges, left (l), right (r), top (t), and bottom (b), are each considered point scatterers, psl1, pst1, psr1, and psb. In the G1 case reflections from only three point scatterers are included plus the large reflection from the substrate surface. This model could be extended to allow for defocused reflections of the edge point scatterers from the substrate, psl2, psr2, and pst2. (d) Model G1.1 could be used for a G2 groove case. The field from a point scatterer is subtracted from a plane reflection from the substrate surface. In Model G1.2 a second point scatterer could be incorporated at the base. For a wider groove point scatterers could be introduced for the edges.

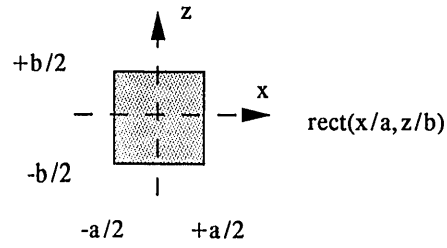

Fig. 13. The step or the groove may be modeled by combinations of two-dimensional rectangular functions as shown.

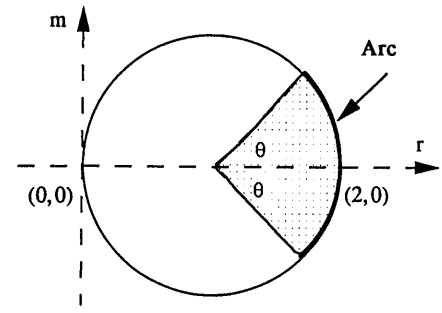

Fig. 14. Two-dimensional Ewald diagram for coherently imaging an object illuminated by a plane wave and collected with a cylindrical lens. All the spatial frequencies in the reflection image lie upon the arc of the shaded sector shown, the ends of which are defined by the N.A. of the lens.

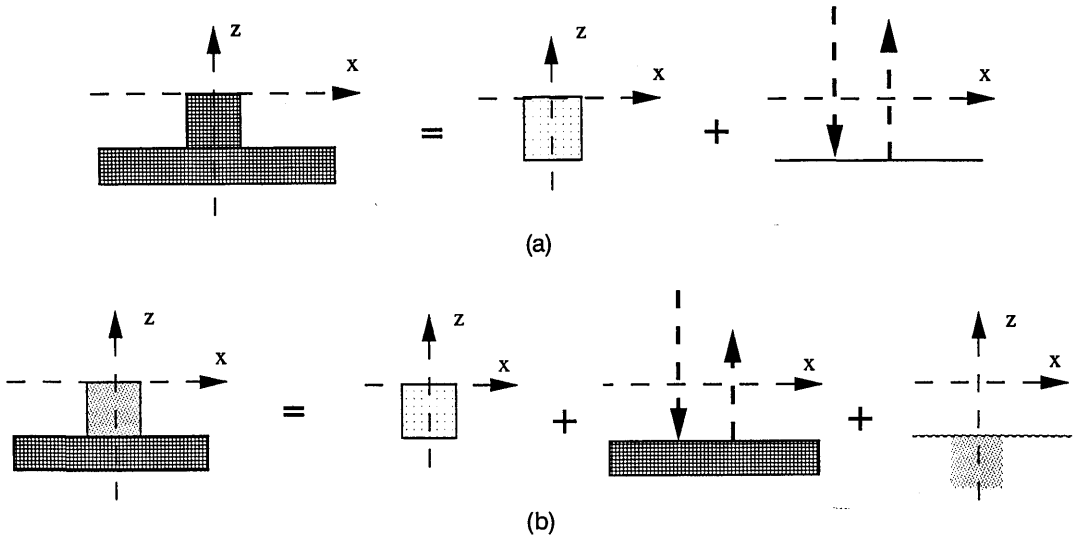

Fig. 15. (a) Model S2.1: For a weakly scattering isolated step, the step being made of the same material as the substrate, the response of the step can be approximated with the two-dimensional Fourier transform of a rectangular scatterer. This response, with the correct phase term, can then be added to the reflection from the substrate. (b) Model S2.2: When the step is made of different material from the substrate, reflections of the scattered field from the substrate must be included. For isolated grooves, the scatter field can be subtracted from the reflection from the substrate.

can be written as

$$I^{(s)}[x, z^{(-)}] = |U^{(s)}[x, z^{(-)}]|^2. \tag{24}$$

The expressions thus calculated can be incorporated into models to calculate the images of isolated steps (Model S2.1), as shown in Fig. 15(a), and can be extended once again, with allowance being made for reflection from the substrate and isolated grooves [Fig. 15(b)]. It should be noted, however, that several limitations on the accuracy of models based on the first Born approximation exist, i.e., no Fabry–Perot effects are incorporated into the rectangular function shown in Fig. 13.

6. CONCLUSIONS

Previous work in the areas of modeling diffraction from dielectric structures and coherent imaging has been discussed. The use of the rigorous modal method to model diffraction by different isolated structures has been presented. The period used for the Fourier series expansion has been examined to ensure the faithfulness of the assumption of noninterference of adjoining isolated structures. The diffracted orders for coherent, normally incident radiation from two common grating forms have been presented and examined for the variation of several physical parameters. Convergence of the results with variations of the number of modes included, N, has been ensured, and the numerical limitations of the rigorous method discussed. Although the implementation appears to give good results, it is felt that a more robust numerical method is necessary, in particular in relation to the difficulties encountered in attempting to carry out calculations for the isolated G1 step.

A set of coherent images, including bright and dark field images, has been calculated, and an examination of the effects of defocus and change of the numerical aperture upon the results has been made. The results have shown that the systematic use of a combination of defocused bright field and dark field images, including an examination of the individual intensities of the diffraction orders, can produce sufficient metrological information to specify the isolated structures. Finally, several first-order approximate models have been suggested that may prove useful in predicting and analyzing diffraction by small isolated phase structures.

ACKNOWLEDGMENTS

J. T. Sheridan thanks the British Council, the Prendergast Fund, and Jesus College, Oxford, for their kind financial assistance. This work was completed while he held an Alexander von Humboldt Fellowship in the Physikalisches Institut of the University of Erlangen-Nurnberg.

*Present address, Department of Physical Optics, School of Physics, The University of Sydney, NSW 2006, Australia.

REFERENCES

1. G. Stagaman and J. M. Forsyth, "Bright-field microscopy of semitransparent objects," J. Opt. Soc. Am. A **5,** 648–659 (1988).
2. T. Wilson and C. J. R. Sheppard, *Theory and Practise of Scanning Optical Microscopy* (Academic, London, 1984).
3. G. S. Kino, C-H. Chou, and G. Q. Xiao, "Imaging theory for the scanning optical microscope," in *Scanning Imaging,* T. Wilson, ed., Proc. Soc. Photo-Opt. Instrum. Eng. **1028,** 104–113 (1988).
4. J. W. Dockrey, "The application of coherence probe microscopy for submicron critical dimension linewidth measurement," in *Integrated Circuit Metrology, Inspection, and Process Control III,* K. M. Monahan, ed., Proc. Soc. Photo-Opt. Instrum. Eng. **1087,** 120–137 (1989).
5. R. Petit, *Electromagnetic Theory of Gratings,* Vol. 22 of Topics in Current Physics (Springer-Verlag, New York, 1980).
6. D. Maystre, "Rigorous vector theories of diffraction gratings," in *Progress in Optics XXII,* E. Wolf, ed. (Elsevier, Amsterdam, 1984), pp. 1–67.
7. H. L. Bertoni, L. S. Cheo, and T. Tamir, "Frequency-selective

reflection and transmission by a periodic dielectric layer," IEEE Trans. Antennas Propag. **37,** 78–83 (1989).
8. J. Y. Suratteau, M. Cadilhac, and R. Petit, "Sur la determination numerique des efficacties de certains reseaux dielectriques profonds," J. Opt. (Paris) **14,** 273–288 (1983).
9. Y. Nakata and M. Koshiba, "Boundary-element analysis of plane-wave diffraction from groove-type dielectric and metallic gratings," J. Opt. Soc. Am. A **7,** 1494–1502 (1990).
10. C. B. Burckhardt, "Diffraction of a plane wave at a sinusoidal stratified dielectric grating," J. Opt. Soc. Am. **56,** 1502–1509 (1966).
11. M. G. Moharam and T. K. Gaylord, "Diffraction analysis of dielectric surface-relief gratings," J. Opt. Soc. Am. **72,** 1385–1392 (1982).
12. J. T. Sheridan and C. J. R. Sheppard, "An examination of the theories for the calculation of diffraction by square-wave gratings: 1. Thickness and period variations for normal incidence," Optik **85,** 25–32 (1990).
13. D. Nyyssonen, "Theory of optical detection and imaging of thick layers," J. Opt. Soc. Am. **72,** 1425–1436 (1982).
14. F. G. Kaspar, "Diffraction by thick, periodically stratified gratings with complex dielectric constant," J. Opt. Soc. Am. **63,** 37–45 (1973).
15. C. P. Kirk and D. Nyyssonen, "Modeling the optical microscope images of thick layers for the purpose of linewidth measurement," in *Optical Microlithography IV,* H. L. Stover, ed., Proc. Soc. Photo-Opt. Instrum. Eng. **538,** 179–187 (1985).
16. D. Nyyssonen and C. P. Kirk, "Optical microscope imaging of lines patterned in thick layers with variable edge geometry: theory," J. Opt. Soc. Am. A **5,** 1270–1280 (1988).
17. B. Richards and E. Wolf, "Electromagnetic diffraction in optical systems II. Structure of the image field in an aplanatic system," Proc. R. Soc. London Ser. A **253,** 358–379 (1959).
18. C. Yuan and A. Strojwas, "Modeling optical microscope images of integrated-circuit structures," J. Opt. Soc. Am. A **8,** 778–790 (1991).
19. J. T. Sheridan and C. J. R. Sheppard, "An examination of the theories for the calculation of diffraction by square-wave gratings: 2. Angular variation," Optik **85,** 57–66 (1990).
20. J. T. Sheridan and C. J. R. Sheppard, "An examination of the theories for the calculation of diffraction by square-wave gratings: 3. Approximate theories," Optik **85,** 135–152 (1990).
21. C. J. R. Sheppard and J. T. Sheridan, "Micrometrology of thick structures," in *Optical Storage and Scanning Technology,* T. Wilson, ed., Proc. Soc. Photo-Opt. Instrum. Eng. **1139,** 32–39 (1989).
22. R. M. Bracewell, *The Fourier Transform and Its Applications* (McGraw-Hill, New York, 1965).
23. T. W. Korner, *Fourier Analysis* (Cambridge U. Press, Cambridge, 1988).
24. K. G. Beauchamp, *A Guide to Signal Processing* (Oxford Science, Oxford, 1987).
25. A. Vasara, E. Nopenen, J. Turunen, J. M. Miller, M. R. Taghizadeh, and J. Tuovinen, "Rigorous diffraction theory of binary optical interconnects," in *Holographic Optics III: Principles and Applications,* G. M. Morris, ed., Proc. Soc. Photo-Opt. Instrum. Eng. **1507,** 224–238 (1991).
26. M. G. Moharam, T. K. Gaylord, G. T. Sincerbox, H. Werlich, and B. Yung, "Diffraction characteristics of photoresist surface-relief gratings," Appl. Opt. **23,** 3214–3220 (1984).
27. M. Born and E. Wolf, *Principles of Optics,* 6th ed. (Pergamon, Oxford, 1980).
28. E. Wolf, "Three-dimensional structure determination of semitransparent objects from holographic data," Opt. Commun. **1,** 153–156 (1969).
29. R. Morf, "Rigorous diffraction theory," Annu. Rep. 26 (Paul Scherrer Institute, Zurich, 1990).
30. R. Morf, Paul Scherrer Institute, Zurich, "Diffraction theory—DOE efficiency," contribution to the Workshop on Optical Information Technology, European Optical Computing Group (received as a personal communication, 1991).
31. D. M. Pai and K. A. Awada, "Analysis of dielectric gratings of arbitrary profiles and thicknesses," J. Opt. Soc. Am. A **8,** 755–762 (1991).
32. K. Knop, "Rigorous diffraction theory for transmission phase gratings with deep rectangular grooves," J. Opt. Soc. Am. **68,** 1206–1210 (1978).
33. A. Lohmann, "An array illuminator based on the Talbot-effect," Optik **79,** 41–45 (1988).
34. C. J. R. Sheppard and H. J. Mathews, "Imaging in high-aperture optical systems," J. Opt. Soc. Am. A **4,** 1354–1360 (1987).
35. I. S. Gradshteyn and I. M. Ryzhik, *Tables of Integrals, Series and Products,* 4th ed. (Academic, New York, 1980).
36. C. J. R. Sheppard and J. M. Heaton, "Images of surface steps in coherent illumination," Optik **68,** 267–280 (1984).
37. C. J. R. Sheppard, "The spatial frequency cut-off in three-dimensional imaging," Part I, Optik **72,** 131–133 (1986); Part II, Optik **74,** 128–129 (1986).
38. P. Beckmann and A. Spizzichino, *The Scatter of Electromagnetic Waves from a Rough Surface* (Artech, Northwood, Mass., 1987).
39. D. J. Wombell and J. A. DeSanto, "Reconstruction of rough-surface profiles with the Kirchhoff approximation," J. Opt. Soc. Am. A **8,** 1892–1897 (1991).